



Research paper

Nitroarene and dye reduction with 2:1 Co/Al layered double hydroxide catalysts – Is gold still necessary?

Sónia R. Leandro^a, Inês J. Marques^a, Ruben S. Torres^a, Tiago A. Fernandes^{b,c}, Pedro D. Vaz^{d,e}, Carla D. Nunes^{a,*}

^a Centro de Química Estrutural, Faculdade de Ciências da Universidade de Lisboa, 1749-016 Lisboa, Portugal

^b Centro de Química Estrutural, Instituto Superior Técnico, Universidade de Lisboa, 1049-001 Lisboa, Portugal

^c Centro de Química e Bioquímica, Faculdade de Ciências da Universidade de Lisboa, 1749-016 Lisboa, Portugal

^d CICECO – Aveiro Institute of Materials, Department of Chemistry, University of Aveiro, 3810-193 Aveiro, Portugal

^e Champalimaud Foundation, Champalimaud Centre for the Unknown, 1400-038 Lisboa, Portugal



ARTICLE INFO

Keywords:

Gold nanoparticles
Hydrotalcite
Dyes
Nitroaromatic compounds
Reduction catalysis
Sustainability

ABSTRACT

A 2:1 Co/Al layered double hydroxide (LDH) material was synthesized with Cl⁻ anions intercalated and then anion exchanged with deprotonated methionine. This allowed further immobilization of Au nanoparticles. The catalytic performance of the set of three LDH materials for comparative benchmarking was assessed in the aqueous reduction of nitroaromatic compounds and of rhodamine dyes in the presence of NaBH₄. All catalysts were found to be very active for the nitro-to-amine reduction. The same was observed for the dyes, where reduction rhodamine 6G was faster than that of rhodamine B, for all catalysts.

While the Au-containing catalyst was apparently the one showing the best catalytic activity the LDH with Cl⁻ was found to follow it closely in terms of catalytic performance. In addition, while the LDH catalyst with Au was prone to deactivation by amine products in recycling experiments, the LDH catalyst with Cl⁻ was almost insensitive to that, which is a large advantage. These results showed that using a catalyst based on first-row metals for efficient processes is possible and addresses current sustainable and environmental concerns.

1. Introduction

Developing sustainable and efficient catalytic processes is a major challenge that is still taking its early steps. This quest is a mandatory mission due to environmental concerns focused on the development of cheap catalysts (including green reaction media) while aiming at a lower consumption of natural resources [1–3].

A way to attain this goal is to mimic Nature's processes and so far, it has never stopped to be an inspiration. Nature designs its activity and provides an incredible range of metal-based materials that are readily available and usually cheap. These are commonly metals from the first-row transition series or others such as Mg, Ca, Zn or Al [4,5]. Exploring such field will result in reducing the use of precious metals, which so far are still unrivaled in catalytic performance, but present huge drawbacks from economic and environmental points of view.

Thus, the number of catalysts and catalytic systems based on the cheaper metals is still limited, fostering new frontiers in their

development is compulsory [6].

Layered double hydroxides (LDHs) are among the inorganic materials that have experienced a high development in recent years, owing to their applications in many fields, namely heterogeneous catalysis [7]. These materials are known for their ion exchange capacity, making possible the introduction of adequately functionalized guests [7,8]. The importance of these materials is based on their ability to retain chemical species with electrical charges compatible to those of the layers. LDHs are known for their extreme versatile customization, arising not only from their composition but also from their anion-exchange capacity, where a huge range of possibilities, both organic and inorganic, is virtually infinite. Anion exchange can be achieved by either (i) anion exchange, (ii) co-precipitation and (iii) reconstruction. Independently of the route chosen, contamination from CO₂ must be prevented, due to the ready and persistent incorporation of carbonate anions within the interlayer of LDHs intercalated with anions other than carbonate [7]. Consequently, it is mandatory to use decarbonated and deionized water

* Corresponding author at: Centro de Química Estrutural, Departamento de Química e Bioquímica, Faculdade de Ciências da Universidade de Lisboa, Campo Grande, Ed. C8, 1749-016 Lisboa, Portugal.

E-mail address: cmnunes@fc.ul.pt (C.D. Nunes).

<https://doi.org/10.1016/j.ica.2021.120336>

Received 26 October 2020; Received in revised form 15 February 2021; Accepted 2 March 2021

Available online 9 March 2021

0020-1693/© 2021 Elsevier B.V. All rights reserved.

under inert atmosphere.

Concerning catalytic applications, the use of LDHs can still go much further in this field meeting the sustainability requirements. The versatility of these materials is not restricted to the ion exchange capacity. In fact, the use of LDHs as catalysts is not restricted to their composition or bulk form (powder) either [9–13]. LDH catalysts were engineered as colloidal nanosheets and more recently, as nanoparticles, as monoliths with hierarchical porosity, or as gelled nanoparticles with high concentration, which defined new frontiers for applications of such materials [11,12,15–24].

Increasing research in recent years led to new non-noble metal catalysts capable of carrying out reactions at lower temperatures and pressures with higher selectivity towards the desired products [25]. Cobalt materials have contributed to this quest as demonstrated by the number of published works describing their use in reduction reactions. Several reports have demonstrated the efficient use of Co in the reduction of nitroaromatic compounds to their amine counterparts. For instance, the chemoselective reduction of a set of nitro compounds was reported by Rai and coworkers using a Ni and Co-based nanocatalyst [26]. The reduction reactions were accomplished strictly in aqueous phase using hydrazine as reducing agent and under very mild conditions (room temperature). Although some of the reactions were not very fast, they reached outstanding performance, especially in selectivity. In other reported works, LDH materials have been used as the catalyst or catalyst support towards reduction of 4-nitrophenol [27,28]. In both works the results were excellent with the catalysts being robust enough to be used across several catalytic cycles. More recently, the group of Zhang has reported a similar system where they replaced Mg by Ni with improved results relatively to their previously reported system [29].

The reduction of dye compounds catalyzed by non-noble metals has also been reported. For instance, Kundu and coworkers reported the synthesis of CoO nanowires with excellent activity [30]. Our group has also reported the efficient use of nanoclustered Co/Al LDH materials for the reduction of rhodamine B dye and benchmarked the results against the bulk LDH equivalent [14]. The results showed that while the standard bulk Co/Al LDH reached 48% substrate conversion at 15 min reaction time, the LDH nanocluster reached 98%. The results were even more dramatic only after 1 min of reaction with the conversion reaching 3.4% and 91% for the bulk and nanocluster catalysts, respectively. The measured reaction rate for the nanocluster LDH was 47-fold higher than that of the bulk, while its surface being only 14 times higher [14].

In this work we report a study on the versatility of Co/Al LDH-based catalysts and how they compared with the engineered version holding Au nanoparticles for the aqueous reduction of nitroaromatic compounds and of rhodamine dyes. As will be discussed throughout this work we found that although the catalyst with Au was the best performing one, one of the Co/Al LDH catalysts followed it closely. This evidenced that despite the presence of Au is beneficial it can be avoided with very good results for catalytic applications in the reduction of the above-mentioned substrates.

2. Experimental

2.1. General

All reagents were purchased from Aldrich and used as received. In this work we have used deprotonated *L*-methionine as the intercalating ligand and will be denoted as *met*. HT_{Co/Al}-Cl, and HT_{Co/Al}-*met* materials were synthesized as reported recently by us [9,15]. A biomimetic methodology was used to synthesize the Au nanoparticles (Au_{NP}) as already reported by us as well [9,15]. Detailed experimental and computational procedures alongside XRD powder patterns (Fig. S1) and FTIR (Fig. S2) for precursor materials can be found in the SI material.

2.2. Catalytic reduction of nitroaromatic compounds

The reduction of nitroaromatic compounds by the HT_{Co/Al}-Cl, HT_{Co/Al}-*met* and HT_{Co/Al}-*met*-Au catalysts was conducted in aqueous solution in the presence of NaBH₄. We chose to test 4-nitroaminophenol, 2,6-dinitrophenol and 4-nitroaniline as substrates. The catalytic reactions were carried out using a quartz cuvette with an optical pathlength of 1 cm. Typically, the catalytic reactions were conducted at room temperature (298–303 K) by mixing 200 μL of an aqueous solution of the relevant nitroaromatic substrate (1 mmol/L) with 1.0 mg of the solid catalyst (which dispersed neatly) in a quartz cuvette, and then adding 2.5 mL deionized water to the quartz cuvette and sonicating to mix them evenly (ca. 10 s). Subsequently, 200 μL of freshly prepared NaBH₄ aqueous solution (0.1 mol/L) were added to the above reaction mixture to start the reduction, being monitored using UV–Vis spectroscopy over a scanning range of 250–500 nm. The kinetics of the reactions were followed for 60 min and measured using the absorbance maxima of each tested substrate (see Fig. S3 in SI material for the UV–Vis spectra of neat compounds) by recording the mixture absorbance at regular time intervals with a UV–Vis spectrophotometer from Shimadzu (UV-2450) equipped with a Peltier cell for temperature control. Initial reaction rates were determined by fitting the absorbance vs. time data to Eq. (1):

$$\ln\left(\frac{C}{C_0}\right)_t = -kt + \ln\left(\frac{C}{C_0}\right)_\infty \quad (1)$$

where $\left(\frac{C}{C_0}\right)_t$ and $\left(\frac{C}{C_0}\right)_\infty$ are the relative quantities of the substrate at time *t* and at the end of reaction, respectively and *k* representing the calculated rate.

2.3. Catalytic reduction of rhodamine dyes

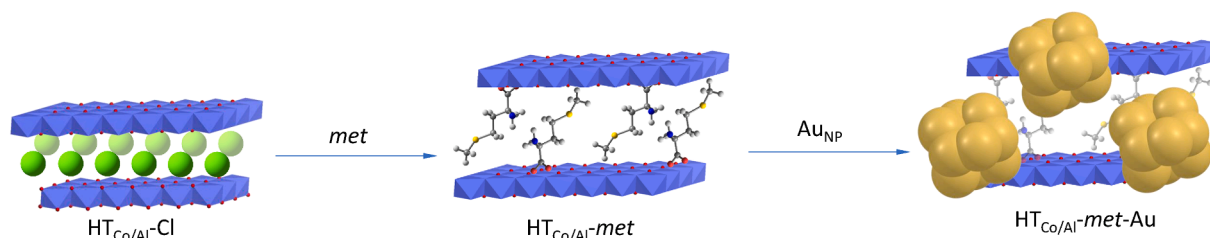
The protocol followed for the reduction of dyes was similar to that described above for the nitroaromatic compounds. Rhodamine B and 6G were chosen as substrates using 20 ppm solutions. In a typical catalytic experiment, 10.0 mg of the solid catalyst were added to 2.5 mL of the 20-ppm aqueous solution of the chosen dye and sonicating for homogeneous dispersion (ca. 10 s). After that, 200 μL of freshly prepared NaBH₄ aqueous solution (0.1 mol/L) were added to the above mixture determining the start of the reduction. The reaction was monitored for 60 min using UV–Vis spectroscopy and scanning across a range between 400 and 700 nm at regular time intervals. The kinetics of the reactions were measured using the absorbance maxima of each substrate tested (see Fig. S4 in SI material for the UV–Vis spectra of neat compounds). The reaction rates were calculated as described above using Eq. (1).

3. Results and discussion

3.1. Synthesis of LDH materials

In this work we have used a combination of co-precipitation and anion exchange methods to prepare clay-based hybrid materials with *L*-methionine (*met*) as evidenced in Scheme 1 [9]. The first step comprised the synthesis of the Co/Al LDH material (denoted as HT_{Co/Al}) synthesized by the co-precipitation method following a reported procedure, as outlined in Scheme 1.

The synthesis produces the carbonate-intercalated material (HT_{Co/Al}-CO₃), which was then ion-exchanged with chloride anions to yield HT_{Co/Al}-Cl [7]. The latter was easier to undergo further ion exchange (due to lower charge density of the Cl[−] anions). Elemental analysis allowed estimation of the chemical composition based on this, the estimated chemical formula was [Co_{0.67}Al_{0.33}(OH)₂][(met)_{0.326}·0.99H₂O] with an experimental Co/Al molar ratio composition of 2.07. The deprotonated *met* amino acid was introduced by ion exchanging the Cl[−] anions [9], yielding the HT_{Co/Al}-*met* material. of the



Scheme 1. Synthetic procedure for preparation of clay materials.

LDH material.

Further reaction of $\text{HT}_{\text{Co/Al}}\text{-met}$ with the gold nanoparticles (Au_{NP}) yielded the new $\text{HT}_{\text{Co/Al}}\text{-met-Au}$ hybrid material. The Au loading was found to be 0.116 wt-% corresponding to $5.9 \times 10^{-3} \text{ mmol}_{\text{Au}} \text{g}^{-1}$ (or $1.2 \text{ mg}_{\text{Au}} \text{g}^{-1}$) for this material.

Electronic spectroscopy (using both absorption and diffuse reflectance techniques) was used to assess formation of the Au-containing hybrid material. $\text{HT}_{\text{Co/Al}}\text{-met-Au}$, whose measured spectra are shown in Fig. 1.

The measured spectrum showed that the $\text{HT}_{\text{Co/Al}}\text{-met-Au}$ material displayed the surface plasmon resonance band at comparable wavelengths to those observed for the as-synthesized Au_{NP} , indicating the successful formation of the $\text{HT}_{\text{Co/Al}}\text{-met-Au}$ material [9,15]. Moreover, the measured absorbance maxima of the hybrid material also changed, which probed the interaction between the Au_{NP} and the host $\text{HT}_{\text{Co/Al}}\text{-met}$ material [9,15]. The surface plasmon resonance band shifted to 565 nm and the methionine bands blue-shifted from 631 and 671 nm (in neat methionine) to 611 and 665 nm, respectively, confirming specific interactions between Au_{NP} and methionine in the $\text{HT}_{\text{Co/Al}}\text{-met-Au}$ material.

Fig. 2 shows the powder XRD patterns of the $\text{HT}_{\text{Co/Al}}\text{-met}$ and $\text{HT}_{\text{Co/Al}}\text{-met-Au}$ materials. Both materials displayed a series of well-developed Bragg reflections in the range $4^\circ < 2\theta < 70^\circ$, which could be indexed to the hexagonal layered LDH structure with rhombohedral symmetry [31]. No peaks from impurities were detected, indicating the high purity of the products.

A set of intense peaks due to basal $00l$ reflections at low 2θ angles allowed us to estimate directly the normal basal spacing to the 001 plane, which is equal to the thickness of one layer of the brucite

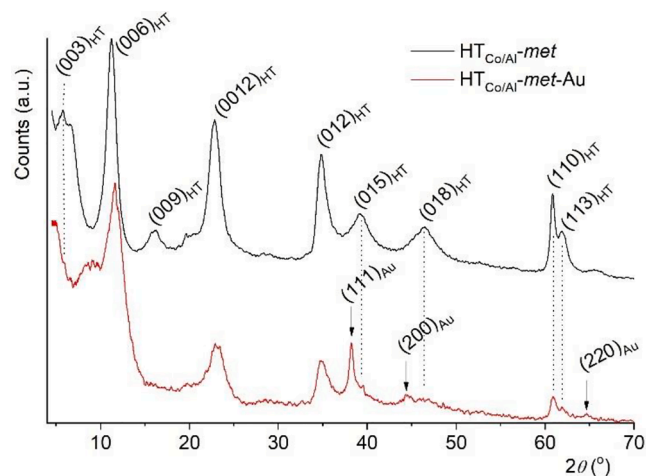


Fig. 2. XRD powder patterns of $\text{HT}_{\text{Co/Al}}\text{-met}$ and $\text{HT}_{\text{Co/Al}}\text{-met-Au}$. The peak at $2\theta = 5.74^\circ$ was assigned to the 003 diffraction peak corresponding to the interlayer space containing the methionine guests. Diffraction peaks arising from Au_{NP} in $\text{HT}_{\text{Co/Al}}\text{-met-Au}$ are highlighted with an arrow at $2\theta = 38.2^\circ$, 44.4° and 64.6° . Diffraction patterns have been offset vertically for clarity.

structure (ca. 4.8 \AA) plus the thickness of the interlayer region [32]. The calculated d parameter was calculated from the second 2θ value corresponding to the 003 plane and found to be 15.30 and 15.20 \AA for both the $\text{HT}_{\text{Co/Al}}\text{-met}$ and $\text{HT}_{\text{Co/Al}}\text{-met-Au}$ materials, respectively. Assuming HT layers (brucite layers) to be 4.8 \AA thick [33,34], the gallery height for $\text{HT}_{\text{Co/Al}}\text{-met}$ was estimated to be 10.5 \AA , indicating that the guest met molecules were most probably in a tilted position.

In addition, other relevant lattice parameters to describe the unit cell were calculated from the 003 and 110 diffraction peaks for both materials, as shown in Table 1 [35,36].

The shortest distance between two cations in one hydroxide layer, $a = 2d_{110}$, is also an important lattice parameter, with both materials displaying the same value ($a = 3.04 \text{ \AA}$). From the d_{003} value, the unit cells ($c = 3d_{003}$) could be calculated showing values of 45.90 and 45.60 \AA

Table 1
Structural parameters for $\text{HT}_{\text{Co/Al}}\text{-met}$ and $\text{HT}_{\text{Co/Al}}\text{-met-Au}$ materials determined by XRD in solid state.

Material	Peak position ^a (°)		Structural parameters (Å)				
	003	110	d_{003}^b	d_{110}^b	a^c	c^d	v^e
$\text{HT}_{\text{Co/Al}}\text{-met}$	5.80	60.85	15.30	1.52	3.04	45.90	119.04
$\text{HT}_{\text{Co/Al}}\text{-met-Au}$	5.80	60.90	15.20	1.52	3.04	45.60	133.89

^a Measured on the XRD powder pattern; ^b d -spacing, calculated with Bragg equation, $n\lambda = 2d\sin\theta_B$, where n is an integer (in general 1), λ is the wavelength of the radiation ($\text{Cu K}\alpha = 1.5405 \text{ \AA}$), d is the lattice spacing and θ_B is the Bragg angle; ^c Shortest distance between two cations in the layer and $a = 2d_{110}$; ^d Unit cell width, $c = 3d_{003}$; ^e Average particle thickness, calculated with Scherrer equation, $v = (K\lambda)/(\beta\cos\theta_B)$, where K is the shape factor (0.89 was used in the calculation), λ is the wavelength of the radiation ($\text{Cu K}\alpha = 1.54 \text{ \AA}$) and β is the 110 peak full width at half maximum in radian.

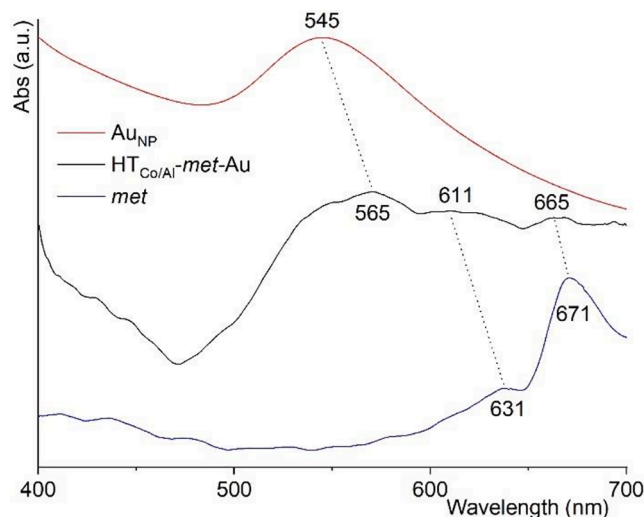


Fig. 1. Electronic spectra of gold nanoparticles (Au_{NP}), methionine (met), and of the hybrid clay material $\text{HT}_{\text{Co/Al}}\text{-met-Au}$. The spectrum of the hybrid materials was obtained as diffuse reflectance (DRUV) while the remaining were obtained from aqueous solutions in transmission mode. Spectra have been offset vertically for clarity.

Å, respectively, for $\text{HT}_{\text{Co/Al}}\text{-met}$ and $\text{HT}_{\text{Co/Al}}\text{-met-Au}$ materials. Moreover, the average thickness of the particles (ν) along the c axis was found to be 119.04 and 133.89 Å for $\text{HT}_{\text{Co/Al}}\text{-met}$ and $\text{HT}_{\text{Co/Al}}\text{-met-Au}$, respectively. Given that a brucite layer is 4.8 Å thick, this suggested that the particles were constituted by ca. 24–28 brucite-like hydroxide layers. These results confirmed that the adopted synthesis procedure of $\text{HT}_{\text{Co/Al}}\text{-met}$ and $\text{HT}_{\text{Co/Al}}\text{-met-Au}$ materials did not alter the primitive structure of the layered double hydroxide.

Peaks due to the presence of the Au_{NP} structures in the $\text{HT}_{\text{Co/Al}}\text{-met-Au}$ material were identified at $2\theta = 38.2^\circ$, 44.4° and 64.6° (Fig. 2, arrow markers).

Diffuse reflectance infrared spectroscopy (DRIFT) was used to characterize all the materials, as shown in Fig. 3.

The FTIR spectra of $\text{HT}_{\text{Co/Al}}\text{-Cl}$, $\text{HT}_{\text{Co/Al}}\text{-met}$ and $\text{HT}_{\text{Co/Al}}\text{-met-Au}$ (Fig. 3a) showed similar profiles. All materials showed a band centered at ca. 3440 cm^{-1} being assigned to the $\nu\text{O-H}$ mode of hydroxyl groups, while the presence of a shoulder at ca. 3150 cm^{-1} suggested that water molecules were interacting with other species by hydrogen bonding. Remaining bands below 800 cm^{-1} may be associated with metal–oxygen bonds in the structure of the clay [15]. The spectrum of the $\text{HT}_{\text{Co/Al}}\text{-met}$

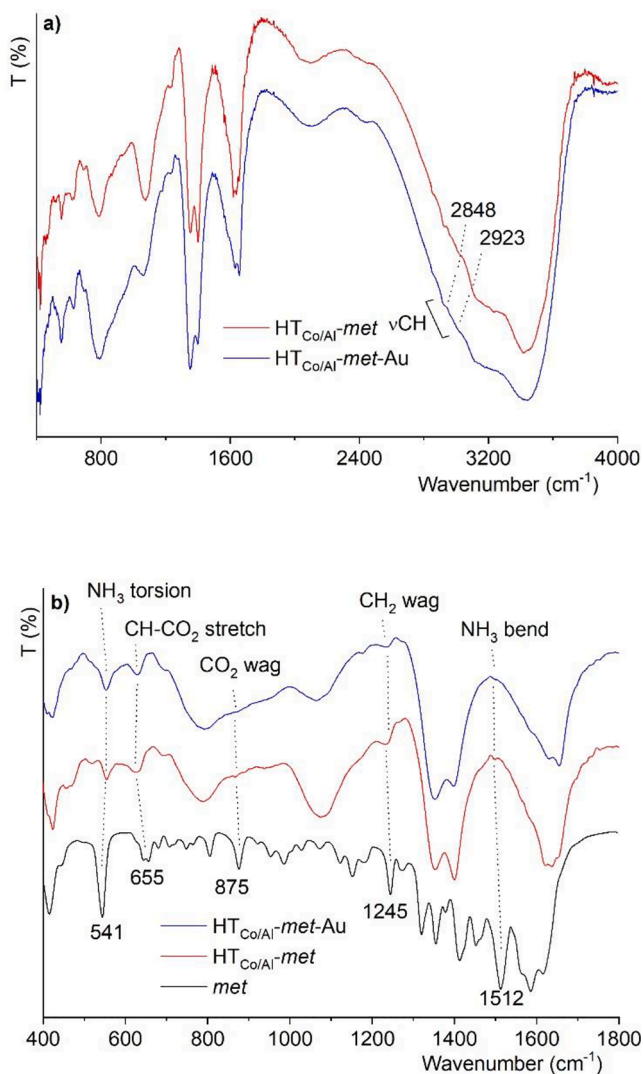


Fig. 3. DRIFT spectra of $\text{HT}_{\text{Co/Al}}\text{-met}$ and $\text{HT}_{\text{Co/Al}}\text{-met-Au}$ materials. In (a) the full spectra are shown. The νCH bands of met in the spectra of $\text{HT}_{\text{Co/Al}}\text{-met}$ and $\text{HT}_{\text{Co/Al}}\text{-met-Au}$ materials were marked for clearer identification. Spectra in (b) display the fingerprint region (modes below 2000 cm^{-1}) of the hybrid materials; the spectrum of met was included for comparison. Spectra in both figures have been offset vertically for clarity.

material allowed identification of a set of bands assigned to the $\nu\text{C-H}$, $\nu\text{C-O}$ and $\nu\text{C=O}$ modes of the methionine amino acid moiety (Fig. 3b).

Unfortunately, bands corresponding to $\nu\text{N-H}$ vibrational modes, expected in the $3300\text{--}3500\text{ cm}^{-1}$ range could not be observed due to overlapping. By the same token, $\nu\text{C-N}$ modes, expected between 1020 and 1220 cm^{-1} were not observed as well due to overlap of the $\nu\text{C-O}$ modes. The characteristic band of lamella hydroxyl groups bound to the metals, $\nu\text{M-O}$ modes, appears near 600 cm^{-1} in the form of a broad band.

Thermogravimetric analysis (TGA) also confirmed the intercalation of met in the interlayer spacing of the HT LDH material. According to Fig. 4, severe decomposition of met was observed at temperatures in the $500\text{--}650\text{ K}$ range. Afterwards, decomposition continues at a slower pace till an overall mass loss of ca. 96.8% at 1073 K .

In the case of $\text{HT}_{\text{Co/Al}}\text{-met}$ its decomposition profile evidenced a mass loss of 12% till ca. 493 K , which was probably due to both adsorbed and intercalated water. The material further decomposed in a two-step way till 1073 K , yielding a total weight loss of 25%. One could assume that met was the sole contributor for the observed weight loss. However, one should still bear in mind that at higher temperature some dehydroxylation was likely to occur and therefore the observed weight loss may arise from decomposition of both moieties. The decomposition profile should be commented as well; in this case the profile was different from that observed for neat met , which could be a proof that met was indeed intercalated within the interlayer spacing of the HT host and therefore protected against thermal decomposition due to specific host–guest interactions [9,15]. The thermal decomposition profile observed for the $\text{HT}_{\text{Co/Al}}\text{-met-Au}$ material was found to superimpose that of the precursor $\text{HT}_{\text{Co/Al}}\text{-met}$ material. This evidenced that the introduction of the Au_{NP} moieties did not induce further changes to the $\text{HT}_{\text{Co/Al}}\text{-met}$ material.

3.2. Catalytic studies on reduction of nitro- to amino-aromatic compounds

It is known that Au and/or Co catalysts can be used as efficient catalysts in reduction reactions [21–24,30]. In this way we tested the set of three clays reported here in the reduction of nitro-aromatic compounds to their amine counterparts. To accomplish this the chosen substrates were p -nitrobenzylalcohol, p -nitroaniline and 2,6-dinitrophenol.

The set of three nitro-aromatic compounds was chosen as to contain model substrates to test the efficiency of the LDH materials in the catalytic reduction of those compounds to their corresponding amine products, in the presence of NaBH_4 . The set of substrates also allowed to

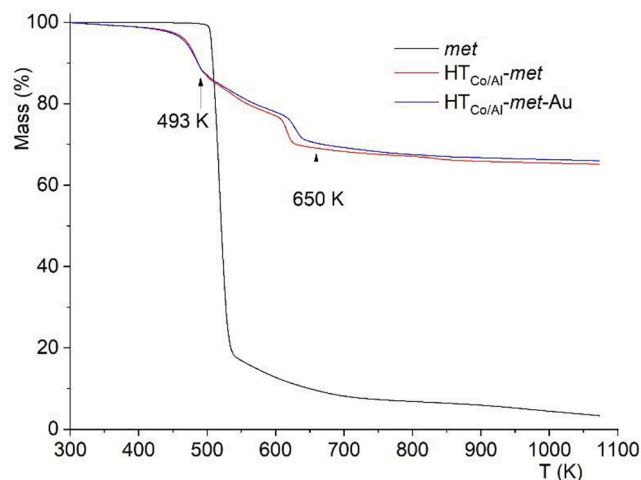


Fig. 4. TGA profiles obtained under N_2 atmosphere at 10 K/min of met , $\text{HT}_{\text{Co/Al}}\text{-met}$ and $\text{HT}_{\text{Co/Al}}\text{-met-Au}$.

screen the catalyst for its chemoselectivity and scope of the reaction. The set of LDH materials allowed benchmarking of their catalytic activity to check whether the presence of the Au_{NP} moieties could be avoided. Furthermore, control reactions with only NaBH_4 in the absence of any catalyst showed almost no effect (after ca. 2 h) on any substrate concentration, confirming that the reduction reaction requires a catalyst.

The results were found to be promising. The reaction kinetics, with reactions being carried out for 60 min, matched [28] or outperformed [26] other systems found in the literature. The use of $\text{HT}_{\text{Co}/\text{Al}}\text{-met-Au}$ as catalyst yielded the desired amine products under *green chemistry* conditions: room temperature (298 K) and water as the reaction medium. The use of NaBH_4 is also environmentally friendly as its decomposition yields NaBO_4 [24].

Fig. 5 shows the UV–Vis kinetics with the substrate concentration of the different nitro-aromatic compounds during the catalytic reaction. It is worth noting that for all substrates there was a dramatic concentration decrease as the reduction reaction progressed in the presence of the Au catalyst.

However, the Au-containing catalyst was followed closely by the $\text{HT}_{\text{Co}/\text{Al}}\text{-Cl}$ counterpart, whereas the $\text{HT}_{\text{Co}/\text{Al}}\text{-met}$ catalyst was the worst performing one in terms of substrate conversion. In fact, a plausible reason for this may arise from the fact that the *met* moiety in the $\text{HT}_{\text{Co}/\text{Al}}\text{-met}$ catalyst was able to establish H-bond interactions with the substrates and delay the reaction kinetics. This situation was minimized or mitigated in the $\text{HT}_{\text{Co}/\text{Al}}\text{-met-Au}$ catalyst because in this case *met* was interacting with Au_{NP} and could not establish further interactions. In the case of the $\text{HT}_{\text{Co}/\text{Al}}\text{-Cl}$ catalyst the H-bonding situation was not possible and therefore the observed catalytic activity was not biased.

The pseudo first-order kinetic model was applied to evaluate the rate constants for nitro-aromatic reduction, allowing to confirm the above statements, because the concentration of NaBH_4 was much higher (100-fold) than those of the substrates and could be considered constant throughout the reaction. The concentration of the substrates at time t was denoted as C_t , while its initial concentration at $t = 0$ was defined as C_0 . The C_t/C_0 ratio was measured from the relative absorbance intensity (A_t/A_0). The rate constants for nitroarene reduction were calculated to be 0.129 min^{-1} for 2,6-dinitrophenol, 0.122 min^{-1} for *p*-nitrobenzylalcohol and 0.040 min^{-1} for *p*-nitroaniline using the $\text{HT}_{\text{Co}/\text{Al}}\text{-met-Au}$ catalyst (Fig. 5, Table 2). The performance of the catalyst in a recycling experiment with 2,6-dinitrophenol displayed an initial reaction rate of 0.046 min^{-1} . This value was around a third of the reaction rate calculated for the fresh catalyst, which indicated that the catalyst suffered deactivation. On the other hand, the $\text{HT}_{\text{Co}/\text{Al}}\text{-met}$ catalyst despite being the one displaying the lowest substrate conversion presented the lowest initial rate constants overall as well. Surprisingly, the $\text{HT}_{\text{Co}/\text{Al}}\text{-Cl}$ one showed rate constant values close to those calculated for the $\text{HT}_{\text{Co}/\text{Al}}\text{-met-Au}$ as catalyst (Table 2). Despite that the $\text{HT}_{\text{Co}/\text{Al}}\text{-Cl}$ catalyst did not reach such a good substrate conversion as displayed by the latter.

The reduction of 2,6-dinitrophenol did not occur through formation of the 2-amino-6-nitrophenol intermediate, as previously observed for the gold-catalyzed reduction of 2,4-dinitrophenol [22]. In that work by Lin and Doong, reduction of 2,4-dinitrophenol was found to occur by sequential reduction of each nitro group, i.e., with 2-amino-4-nitrophenol as intermediary compound, which was evidenced by the appearance of a new band at early times of the reaction, which vanished with increasing time [22]. In our study we did not observe this behavior according to the measured spectra (not shown). The reason behind this may be that 2,6-dinitrophenol may undergo parallel reduction of both nitro groups to form directly 2,6-diaminophenol in the presence of the Au catalyst and NaBH_4 . This may arise from the favorable geometrical arrangement of its nitro groups, which can bind at the same time to the catalyst's surface.

The mechanism for this Au-catalyzed process should follow that reported in the literature for a related system [23]. The mechanism assumed that the first step comprises the adsorption of BH_4^- ions at the

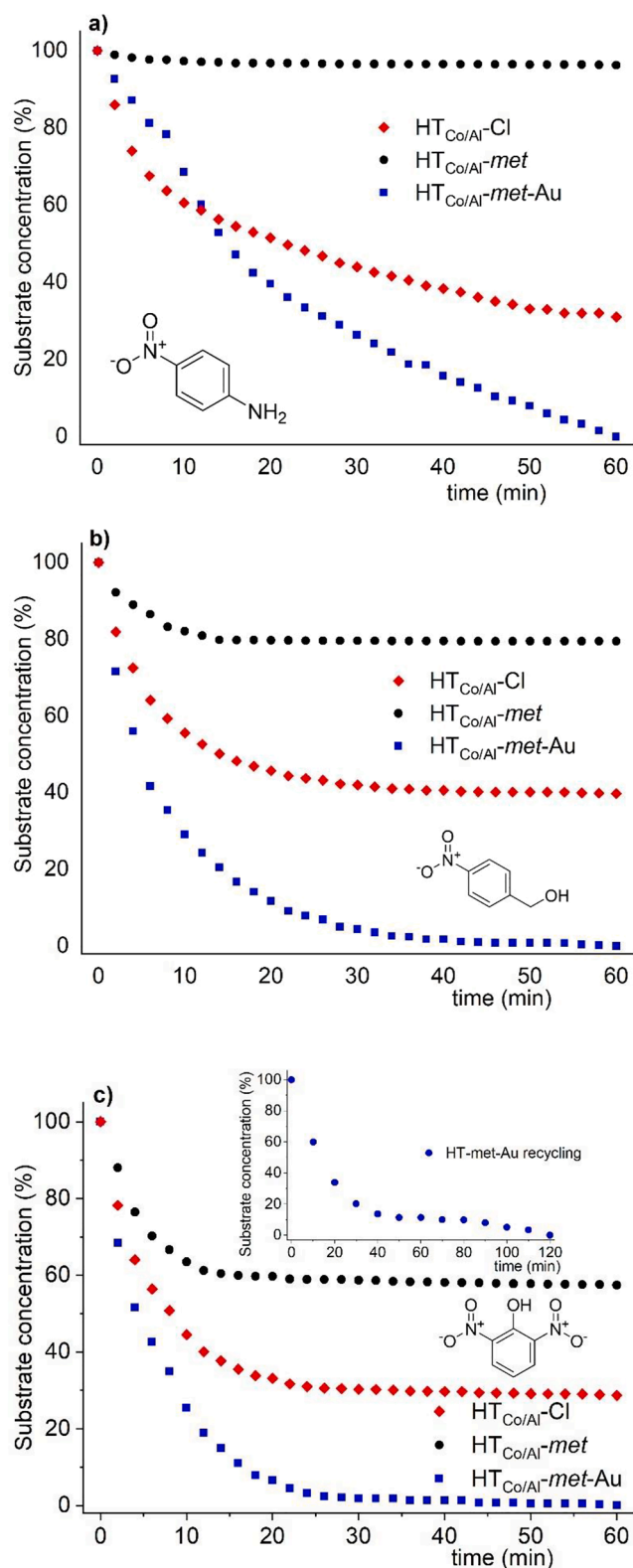


Fig. 5. Time-dependent UV–Vis changes of a) *p*-nitroaniline (375 nm), b) *p*-nitrobenzylalcohol (272 nm) and c) 2,6-dinitrophenol (342 nm). The inset in c) shows the kinetics for the recycling experiment using the $\text{HT}_{\text{Co}/\text{Al}}\text{-met-Au}$ catalyst. Fig. S5 shows the linearized plots of the reaction kinetics data.

Table 2

Catalytic aqueous reduction of nitroaromatic compounds using the set of HT materials as catalysts in the presence of NaBH₄.

Entry	Substrate	Catalyst ^a	Conversion ^b (%)	k ^c (×10 ³ min ⁻¹)
1		HT _{Co/Al} -Cl	69	50
2		HT _{Co/Al} - <i>met</i>	< 5	14
3		HT _{Co/Al} - <i>met</i>	100	40
4		HT _{Co/Al} -Cl	60	64
5		HT _{Co/Al} - <i>met</i>	21	19
6		HT _{Co/Al} - <i>met</i> -Au	100	122
7		HT _{Co/Al} -Cl	71	78
8		HT _{Co/Al} - <i>met</i>	43	46
9		HT _{Co/Al} - <i>met</i> -Au	100	129/46 ^d

^aAll reactions were carried out in the presence of 1.0 mg of catalyst; ^b Conversion calculated after 60 min. reaction time; ^c Rates calculated according to Eq. (1) (Experimental section); ^d Rate values for the regular (1st) and recycling (2nd) experiments, respectively.

surface of the Au nanoparticles yielding Au-hydride complex. The second step comprises adsorption of the nitroaromatic substrate at the surface of the Au nanoparticles as well. Both steps are reversible thus competing with NH₂ groups (when present) confirming the observation of lower reaction rates in *p*-nitroaniline, as already discussed before [22,23].

After the adsorption, hydrogen transfer takes place sequentially, forming nitroso and hydroxylamine (intermediaries) to finally yield the aniline product. According to literature data [37], the reaction is fast till formation of the hydroxylamine intermediary, but the final step (involving product desorption) to originate the aniline is the rate determining step. The aniline product then desorbs regenerating the catalyst. We believe that a similar mechanism could be used to explain the catalytic activity of the remaining HT_{Co/Al}-Cl and HT_{Co/Al}-*met* catalysts, by hypothesizing that BH₄⁻ ions adsorb at the surface of the mixed-metal oxide sheets, especially at Co sites. In this case the reducing agent was probable to reduce Co(III) loci to Co(II) or Co(0), which in turn will make the catalyst active for the reduction reaction.

It is known that Au catalysts are environment-sensitive to reaction conditions, such as solvent or functional groups – e.g. amine or thiol groups – from other molecules in solution [20]. In this case, we observed that reduction of 2,6-dinitrophenol and *p*-nitrobenzylalcohol displayed higher rate constants than *p*-nitroaniline. This was also evidenced in the recycling experiment of HT_{Co/Al}-*met*-Au in the reduction of 2,6-dinitrophenol (Table 2). According to the literature data, the dramatic decrease in rate constants for *p*-nitrophenol reduction is attributed to the presence of amine products, which then bind to the surface of Au nanoparticles with concomitant deactivation.

To confirm these assumptions, we carried out simple DFT calculations to explore both the amine (using aniline as model compound) and borohydride coordination to gold. The optimized geometries for the resulting gold complexes are shown in Fig. 6.

The formation of both species was predicted to be favorable with their enthalpies being –6.0 and –8.4 kcal mol⁻¹ for the aniline and borohydride complexes, respectively. This result showed that the borohydride complex is the most stable and, therefore, there should be no problem associated with the recycling experiments concerning kinetics. However, the energy difference was found to be small enough to allow both species to coexist at the reaction temperature (ca. 300 K) and compete for Au coordination. This may certainly account for the observed slower kinetics effect when starting with *p*-nitroaniline and in the recycling experiment of 2,6-dinitrophenol.

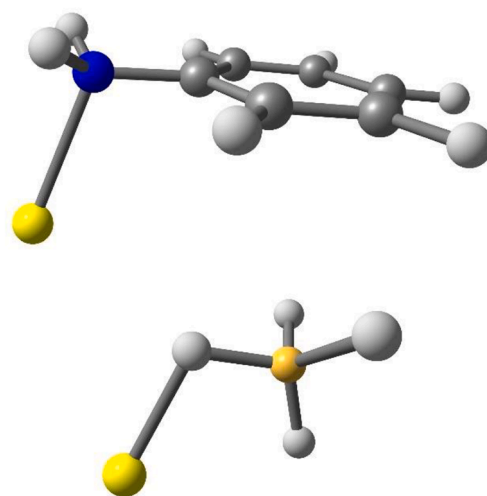


Fig. 6. DFT optimized structures of Au(0) complexes with aniline (top) and borohydride anion (bottom).

3.3. Catalytic studies on reduction of dyes

To evaluate the scope of action of this set of three catalysts, we also tested them in the reduction of dyes. For this study rhodamine B and rhodamine 6G were chosen as the candidates. Overall, the results followed the same trend as that discussed above for the catalytic reduction of the nitro aromatic compounds. According to Fig. 7 the reaction progressed spontaneously as evidenced by the control experiments on both substrates.

However, in the presence of any of the catalysts the reactions were much faster. The observed catalytic performance followed the HT_{Co/Al}-*met* < HT_{Co/Al}-Cl < HT_{Co/Al}-*met*-Au trend. These results were valid for both the substrate conversion as well as for the initial reaction rates as shown in Table 3.

As can be seen, the HT_{Co/Al}-*met* counterpart was the worst performing. An explanation for this may be the same discussed earlier in this work, where the existence of intermolecular H-bonds between the *met* moiety in the HT_{Co/Al}-*met* catalyst and the substrates hindered the reaction kinetics.

Comparing the reaction kinetics between the dye substrates for a given catalyst it was observed that reduction of the rhodamine 6G substrate was always faster than the kinetics for reduction of rhodamine B. This may arise from the slight structural differences presented by both substrates (Table 3). Rhodamine 6G has less bulky amine groups (secondary amine groups) than rhodamine B (tertiary amine groups), which could be more prone for interaction with the reactive sites. This was observed across all catalysts studied in this work.

Most interestingly, the results from the recycling experiments were more exciting. As observed for the reduction of nitroaromatic compounds, the HT_{Co/Al}-*met*-Au catalyst experienced a dramatic decrease of the reaction rate due to deactivation by the presence of the amine moieties. In this case, for rhodamine B the reaction rate was found to decrease from 0.076 to 0.040 min⁻¹ (47% decrease; Table 3, entry 4), while for rhodamine 6G the rate dropped from 0.168 to 0.087 min⁻¹ (48% decrease; Table 3, entry 9).

However, the HT_{Co/Al}-Cl counterpart did not evidence major changes in the reaction rate, showing that this catalyst is not prone to poisoning by the amine moieties, which was a pleasant surprise. With this catalyst, the reaction rate for rhodamine B decreased from 0.069 to 0.053 min⁻¹ (23% decrease; Table 3, entry 1), while for rhodamine 6G the rate changed from 0.182 to 0.116 min⁻¹ (36% decrease; Table 3, entry 5). Overall, these results evidenced that, although achieving similar substrate conversion, the HT_{Co/Al}-Cl catalyst was the best performing one given that it experienced less deactivation in the recycling

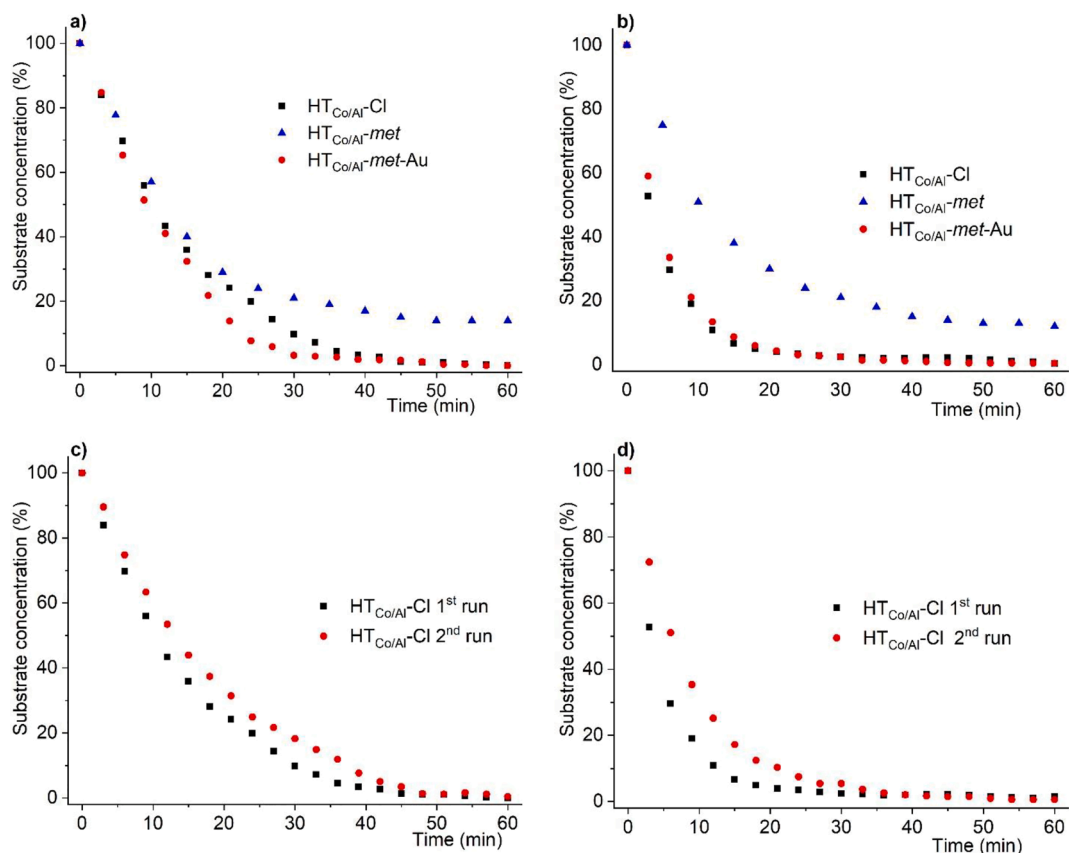


Fig. 7. Time-dependent UV-Vis changes of rhodamine B (554 nm, *a* and *c*) and rhodamine 6G (526 nm, *b* and *d*) in the presence of the $\text{HT}_{\text{Co/Al-Cl}}$, $\text{HT}_{\text{Co/Al-met}}$ and $\text{HT}_{\text{Co/Al-met-Au}}$ catalysts. The plots in *c*) and *d*) show the kinetics for two consecutive catalytic reduction reactions of rhodamine B (*c*) and rhodamine 6G (*d*) in the presence of $\text{HT}_{\text{Co/Al-Cl}}$ evidencing its little sensitivity to deactivation. Fig. S7 shows the linearized plots of the reaction kinetics data.

Table 3

Catalytic aqueous reduction of rhodamine B and 6G dyes using the set of HT materials as catalysts in the presence of NaBH_4 .

Entry	Substrate	Catalyst ^a	Conversion ^b (%)	k^c ($\times 10^3 \text{ min}^{-1}$)
1		$\text{HT}_{\text{Co/Al-Cl}}$	100	69/53 ^e
2		$\text{nanoHT}_{\text{Co/Al-Cl}}$	100 ^d	2100 ^d
3		$\text{HT}_{\text{Co/Al-met}}$	86	64
4		$\text{HT}_{\text{Co/Al-met-Au}}$	100	76/40 ^e
5		$\text{HT}_{\text{Co/Al-Cl}}$	100	182/116 ^e
6		$\text{HT}_{\text{Co/Al-met}}$	88	76
7		$\text{HT}_{\text{Co/Al-met-Au}}$	100	168/87 ^e

^aAll reactions were carried out in the presence of 1.0 mg of catalyst; ^b Conversion calculated after 60 min. reaction time; ^c Rates calculated according to Eq. (1) (Experimental section); ^d results from ref. [14] after 15 min; ^e Rate values for the regular (1st) and recycling (2nd) experiments, respectively.

experiment.

Compared to literature data for a related nanosized catalyst (**nano-HT_{Co/Al}**) recently reported by us, the one reported here (bulk form) is much less active concerning the reaction kinetics (by ca. 30-fold, [Table 3](#), entries 1 and 2) [14]. However, the substrate conversion was also found to be the same, reaching reaction completeness with the difference that the reaction times were 15 and 60 min., respectively for the **nanoHT_{Co/Al}** and **HT_{Co/Al-Cl}** catalysts.

Finally, we have also studied eventual structural changes suffered by the catalysts after catalysis. In this way, we measured the XRD powder pattern for a **HT_{Co/Al-met-Au}** catalyst sample recovered after two consecutive Rh6G reduction reactions and found that the overall profile was kept ([Fig. S8](#) in SI material), demonstrating that these catalysts were robust. It should be worth mentioning that Au loading after these two reactions decreased by 19%.

4. Conclusions

In this work we reported the preparation of a set of Co/Al LDH materials with increasing complexity. All of them were successfully tested as catalysts for the reduction of nitroaromatic compounds and dyes. The best performance was obtained with the one holding Au nanoparticles. The DFT calculations demonstrated that there was competition between amine moieties and borohydride, which explained the deactivation of the Au catalyst in the recycling experiments. However, the simplest catalyst, **HT_{Co/Al-Cl}** presented catalytic activity close to the Au-containing counterpart. This opened a window of opportunity to take further steps in exploring this system for those reactions. In addition, this also demonstrated that efforts to prepare sustainable and environmentally friendly catalysts such as those reported here are promising viable options. Therefore, as exhibited by the results obtained for **HT_{Co/Al-Cl}**, based on first-row *d*-block elements, it was demonstrated that noble and expensive metals can be avoided and replaced conveniently. Moreover, the reactions herein reported were conducted in aqueous phase, which showed that these systems did not pose any environmental pressure concerns in terms of residues.

Recycling experiments also demonstrated that although the Au catalyst was prone to deactivation by amine products in recycling experiments, the **HT_{Co/Al-Cl}** catalyst seemed to be almost insensitive to that. It is a remarkable feature of this catalyst.

Therefore, excellent perspectives for future developments of this system, which are being endeavored by us, can be foreseen.

CRedit authorship contribution statement

Sónia R. Leandro: Investigation, Formal analysis. **Inês J. Marques:** Investigation, Formal analysis, Writing - review & editing. **Ruben S. Torres:** Investigation, Formal analysis. **Tiago A. Fernandes:** Investigation, Formal analysis, Writing - review & editing. **Pedro D. Vaz:** Conceptualization, Investigation, Data curation, Writing - review & editing. **Carla D. Nunes:** Conceptualization, Methodology, Supervision, Project administration, Writing - review & editing.

Declaration of Competing Interest

The authors declare that they have no known competing financial interests or personal relationships that could have appeared to influence the work reported in this paper.

Acknowledgments

The authors would like to acknowledge FCT for financial support

(projects UIDB/00100/2020 and UIDP/00100/2020). TAF thanks CQB and FCT for a fellowship (PEst-OE/MULTI/00612/2013 and CEECIND/02725/2018).

Appendix A. Supplementary data

Supplementary data to this article can be found online at <https://doi.org/10.1016/j.ica.2021.120336>.

References

- [1] D. Astruc, *Nanoparticles and Catalysis*, Wiley, Weinheim, 2008.
- [2] R.J. White, R. Luque, V.L. Budarin, J.H. Clark, D.J. Macquarrie, *Chem. Soc. Rev.* **38** (2009) 481–494.
- [3] L. Mai, F. Yang, Y. Zhao, X. Xu, L. Xu, B. Hu, Y. Luo, H. Liu, *Mater. Today* **14** (2011) 346–353.
- [4] [4] European Cluster on Catalysis, Science and Technology Roadmap on Catalysis for Europe, http://www.catalysiscluster.eu/wp/wp-content/uploads/2017/01/Science-and-Technology-Roadmap-on-Catalysis-2016_Edited-Version-with-ISBN-1.pdf, 2016 (accessed 15 February 2021).
- [5] G. Arrabito, R. Pezilli, G. Prestopino, P.G. Medaglia, *Crystals* **10** (2020) 602.
- [6] [6] SPIRE, SPIRE Roadmap, www.spire2030.eu/sites/default/files/pressoffice/spire-roadmap.pdf, 2019 (accessed 15 February 2021).
- [7] C.I. Fernandes, C.D. Nunes, P.D. Vaz, *Curr. Org. Synth.* **9** (2012) 670–694.
- [8] A.R. Sotiles, L.M. Baika, M.T. Grassi, F. Wypych, *J. Am. Chem. Soc.* **141** (2019) 531–540.
- [9] S.R. Leandro, C.I. Fernandes, A.S. Viana, A.C. Mourato, P.D. Vaz, C.D. Nunes, *Appl. Catal. A: Gen.* **584** (2019), 117155.
- [10] Y. Tokudome, N. Tarutani, K. Nakanishib, M. Takahashia, *J. Mater. Chem. A* **1** (2013) 7702–7708.
- [11] N. Tarutani, Y. Tokudome, M. Fukui, K. Nakanishi, M. Takahashi, *RSC Adv.* **5** (2015) 57187–57192.
- [12] Y. Tokudome, T. Morimoto, N. Tarutani, P.D. Vaz, C.D. Nunes, V. Prevot, G.B. G. Stenning, M. Takahashi, *ACS Nano* **10** (2016) 5550–5559.
- [13] J. Wang, L. Zhao, H. Shi, J. He, *Angew. Chem. Int. Ed.* **5** (2011) 9171–9176.
- [14] D. Kino, Y. Tokudome, P.D. Vaz, C.D. Nunes, M. Takahashi, *J. Asian Ceram. Soc.* **5** (2017) 466–471.
- [15] S.R. Leandro, A. Mourato, U. Łapińska, O.C. Monteiro, C.I. Fernandes, C.D. Nunes, P.D. Vaz, *J. Catal.* **358** (2018) 187–198.
- [16] L. Li, L. Dou, H. Zhang, *Nanoscale* **6** (2014) 3753–3763.
- [17] L. Wang, J. Zhang, X. Meng, D. Zheng, F. Xiao, *Catal. Today* **175** (2011) 404–410.
- [18] J. Wang, X. Lang, B. Zhaorigetu, M. Jia, J. Wang, X. Guo, J. Zhao, *ChemCatChem* **6** (2014) 1737–1747.
- [19] X. Wang, G. Wu, F. Wang, K. Ding, F. Zhang, X. Liu, Y. Xue, *Catal. Commun.* **28** (2012) 73–76.
- [20] S. Nakagaki, M. Halma, A. Bail, G.G.C. Arizaga, F. Wypych, *J. Colloid Interf. Sci.* **281** (2005) 417–423.
- [21] X. Bai, Y. Gao, H. Liu, L. Zheng, *J. Phys. Chem. C* **113** (2009) 17730–17736.
- [22] F. Lin, R. Doong, *J. Phys. Chem. C* **115** (2011) 6591–6598.
- [23] K. Layek, M.L. Kantam, M. Shirai, D. Nishio-Hamane, T. Sasaki, H. Maheswaran, *Green Chem.* **14** (2012) 3164–3174.
- [24] H.K. Kadam, S.G. Tilve, *RSC Adv.* **5** (2015) 83391–83407.
- [25] D. Formenti, F. Ferretti, F.K. Scharnagl, M. Beller, *Chem. Rev.* **119** (2019) 2611–2680.
- [26] R.K. Rai, A. Mahata, S. Mukhopadhyay, S. Gupta, P.-Z. Li, K.T. Nguyen, Y. Zhao, B. Pathak, S.K. Singh, *Inorg. Chem.* **53** (2014) 2904–2909.
- [27] L. Dou, H. Zhang, *J. Mater. Chem. A* **4** (2016) 18990–19002.
- [28] N. Arora, A. Mehta, A. Mishra, S. Basu, *Applied Clay Sci.* **151** (2018) 1–9.
- [29] Z. Wei, Y. Li, L. Dou, M. Ahmad, H. Zhang, *ACS Appl. Nano Mater.* **2** (2019) 2383–2396.
- [30] S. Kundu, M.D. Mukadam, S.M. Yusuf, M. Jayachandran, *CrystEngComm* **15** (2013) 482–497.
- [31] C. Taviot-Gueho, F. Leroux, C. Payen, J.P. Besse, *Appl. Clay Sci.* **28** (2005) 111–120.
- [32] J.C. Dupin, H. Martinez, C. Guimon, E. Dumitriu, I. Fechete, *Appl. Clay Sci.* **27** (2004) 95–106.
- [33] S.P. Newman, W. Jones, *New J. Chem.* **22** (1998) 105–115.
- [34] S.P. Newman, S.J. Williams, P.V. Coveney, W. Jones, *J. Phys. Chem. B* **102** (1998) 6710–6719.
- [35] C.I. Fernandes, P.D. Vaz, T.G. Nunes, C.D. Nunes, *Applied Clay Sci.* **190** (2020), 105562.
- [36] M. Pavlovic, F. Dits, Z. Gu, M. Adok-Sipiczki, I. Szilagyi, *RSC Adv.* **6** (2016) 16159–16167.
- [37] A. Corma, P. Concepcion, P. Serna, *Angew. Chem.* **119** (2007) 7404–7407.